



## PAPER

## Acousto-elasticity of transversely isotropic incompressible soft tissues: characterization of skeletal striated muscle

RECEIVED  
11 March 2021REVISED  
11 June 2021ACCEPTED FOR PUBLICATION  
29 June 2021PUBLISHED  
13 July 2021Jean-Pierre Remenieras<sup>1,\*</sup> , Mahé Bulot<sup>1</sup>, Jean-Luc Genisson<sup>2</sup> , Frédéric Patat<sup>1,3</sup>, Michel Destradre<sup>4</sup>  and Guillaume Bacle<sup>1,5</sup><sup>1</sup> UMR 1253, iBrain, Université de Tours, Inserm, Tours, France<sup>2</sup> Laboratoire d'imagerie biomédicale multimodale à Paris-Saclay, Université Paris-Saclay, CEA, CNRS UMR 9011, INSERM UMR 1281, France<sup>3</sup> Inserm CIC-IT 1415, Tours, France<sup>4</sup> School of Mathematics, Statistics and Applied Mathematics, NUI Galway, University Road, Galway, Ireland<sup>5</sup> Service de chirurgie orthopédique et traumatologique 1A, Unité de chirurgie de la main et du membre supérieur, CHRU de Tours, France

\* Author to whom any correspondence should be addressed.

E-mail: [jean-pierre.remenieras@univ-tours.fr](mailto:jean-pierre.remenieras@univ-tours.fr)**Keywords:** acousto-elasticity, shear wave elastography, transversely isotropic soft solid, third order elastic constants, musculoskeletal disorders, maximum voluntary contractionSupplementary material for this article is available [online](#)**Abstract**

Using shear wave elastography, we measure the changes in the wave speed with the stress produced by a striated muscle during isometric voluntary contraction. To isolate the behaviour of an individual muscle from complementary or antagonistic actions of adjacent muscles, we select the *flexor digiti minimi* muscle, whose sole function is to extend the little finger. To link the wave speed to the stiffness, we develop an acousto-elastic theory for shear waves in homogeneous, transversely isotropic, incompressible solids subject to an uniaxial stress. We then provide measurements of the apparent shear elastic modulus along, and transversely to, the fibre axis for six healthy human volunteers of different age and sex. The results display a great variety across the six subjects. We find that the slope of the apparent shear elastic modulus along the fibre direction changes inversely to the maximum voluntary contraction (MVC) produced by the volunteer. We propose an interpretation of our results by introducing the S (slow) or F (fast) nature of the fibres, which harden the muscle differently and accordingly, produce different MVCs. A natural follow-up on this study is to apply the method to patients with musculoskeletal disorders or neurodegenerative diseases.

**1. Introduction**

Affecting around 25% of people worldwide, musculoskeletal disorders have a high prevalence in the adult population, coupled to enormous and increasing health and societal impacts (Badley *et al* 1994, Adams and Marano 1995, Woolf and Åkesson 2001, WHO ScientificGroup 2003). Although mainly non-lethal, these pathologies cause significant morbidity with decreased function in daily life activities and lower quality of life (Reginster and Khaltayev 2002, Vos *et al* 2012, Storheim and Zwart 2014). They also generate significant economic costs (Jacobson *et al* 1996, WHO ScientificGroup 2003).

The pathophysiology of many of these disorders is still not completely understood and the development of new diagnostic strategies and bio-markers specific to musculoskeletal tissues is crucial to medical progress (Storheim and Zwart 2014). Also, skeletal, voluntary-controlled, muscles play a big role in motorizing joints, maintaining posture, and regulating peripheral blood flow. Hence, innovative assessments of muscle mechanical properties and dynamics linked to its very specific structural fibrillary organization can improve our understanding of normal and pathological muscle tissue behaviour and strength (Storheim and Zwart 2014, Gijssbertse *et al* 2017).

Over the past twenty years, ultrasound imaging techniques have gained sufficient temporal resolution to become ultra-fast ( $> 1000$  frames  $s^{-1}$ ) and investigate the kinematics of muscle. Hence, they have been used to assess the dynamical behaviour and structural changes of normal and pathological contractile tissues (Miyatake *et al* 1995, Nagueh *et al* 1998, Yeung *et al* 1998, Dh'ooge *et al* 2000, Loram *et al* 2006, Deffieux *et al* 2008a, Lopata *et al* 2010, Eranki *et al* 2013, Downs *et al* 2018).

Nonetheless, the biomechanical characteristics of skeletal muscle remain difficult to clarify fully because of its complex structural organization and its contractile properties (Gennisson *et al* 2010). Indeed, as can be seen to the naked eye, skeletal muscle tissue is composed of families of parallel muscular fibres. Muscle contraction is carried out by the shortening of these fibres, which results from the active sliding of the thick myosin filaments between the fine actin filaments found within the fibres. Therefore, the main biomechanical characteristics of muscle tissue associated with contraction are shortening and hardening (Ford *et al* 1981). Thus, techniques that provide quantitative data on tissue deformation and elastic properties could be of great help in understanding dynamic muscle behaviour. One such technique is quantitative shear wave elastography (SWE), proposed by Sarvazyan *et al* (1998), and then refined and used to quantitatively characterize the mechanical parameters of normal skeletal muscle tissues (Nordez *et al* 2008, Gennisson *et al* 2010, Nordez and Hug 2010, Bouillard *et al* 2011, Koo *et al* 2014, Tran *et al* 2016). Some attempts have also been made to indirectly evaluate muscle forces based on muscle elasticity using SWE (Bouillard *et al* 2011, Hug *et al* 2015, Kim *et al* 2018).

Interestingly, muscle stiffness increases differently with tension during sustained contraction, depending on the type of motor units activated, according to Petit *et al* (1990), who performed measurements in the *peroneus longus* muscle of anesthetized cats. These authors found that the stiffness/tension slope is greater when (slow) S-type motor units are activated, compared to (fast fatigue-resistant) FR-type and (fast fatiguable) FF-type motor units. Their result suggests that S-type motor units contribute more to muscle hardness during contraction than F-type ones, and that the stiffness/tension relationship must consequently change according to the S/F ratio.

During voluntary contraction, an axial stress is induced inside the muscle tissue by the shortening of the fibres which modifies its mechanical properties. The goal of this paper is to measure experimentally the changes in shear wave speed during voluntary contraction on healthy volunteers and to model these changes with the acousto-elasticity theory. This theory couples nonlinear elasticity modelling of materials and elastic wave propagation, and links the wave speed to uni-axial stress using high-order elastic constants. Due to the presence of fibres, muscles are considered as anisotropic, specifically transversely isotropic (TI). It follows that shear waves propagate at different speeds depending on the orientation of the propagation and polarization directions with respect to the fibre axis (Gennisson *et al* 2003). We show in the next section how acousto-elasticity theory can be adapted to study shear wave propagation in an homogeneous TI incompressible solid, subject to a uniaxial stress, extending the available theory for isotropic solids (Gennisson *et al* 2007, Destrade *et al* 2010b). Acousto-elasticity theory links the shear wave speed to the uniaxial stress (Gennisson *et al* 2007) or, equivalently, to the uni-axial elongation (Destrade *et al* 2010b). Both formulations have been used for *in vivo* experiments when the stress is applied directly by pressing the ultrasound probe onto the tissue (Latorre-Ossa *et al* 2012, Bernal *et al* 2015, Jiang *et al* 2015, Bayat *et al* 2019, Ottesteanu *et al* 2019). This approach was also developed for TI media (Bied *et al* 2020). Here we measured the stress directly with a force sensor (Bouillard *et al* 2014) applied on the *flexor digiti minimi* muscle.

## 2. Acousto-elasticity in fibre muscle

### 2.1. Uniaxial stress in incompressible TI solids

We model muscles as soft incompressible materials with one preferred direction, associated with a family of parallel fibres.

TI *compressible* solids are described by five independent constants, for example the following set (Rouze *et al* 2020):  $\mu_L$ ,  $E_L$ ,  $E_T$ ,  $\nu_{LT}$ ,  $\nu_{TT}$ , where  $\mu_L$  is the shear elastic modulus relative to deformations along the fibres,  $E_L$ ,  $E_T$  are the Young moduli along, and transverse to, the fibres, respectively. The Poisson ratios  $\nu_{LT} = -\frac{E_{22}}{E_{11}}$  and  $\nu_{TT} = -\frac{E_{22}}{E_{33}}$  couple the transverse strain  $E_{22}$  to the axial  $E_{11}$  and the transverse  $E_{33}$  strains when stressed in the  $x_1$  and  $x_3$  directions, respectively. The shear elastic modulus  $\mu_T$  relative to the transverse direction is  $\mu_T = \frac{E_T}{2(1 + \nu_{TT})}$ .

For *incompressible* TI materials, there is no volume change. This constraint leads to the following relations (see Rouze *et al* (2020) for details),

$$\nu_{LT} = \frac{1}{2}, \quad \nu_{TT} = 1 - \frac{E_T}{2E_L}. \quad (1)$$

Thus, only three independent constants are required to fully describe a given TI, linearly elastic, incompressible solid. Here we choose the three material parameters  $\mu_T$ ,  $\mu_L$ , and  $E_L$ , as proposed by Li *et al* (2016). Note that other, equivalent choices can be made (Chadwick 1993, Papazoglou *et al* 2006, Rouze *et al* 2013).

We call  $x_1$  the axis along the fibres and  $\sigma_{11}$  the uniaxial stress applied by the volunteers in that direction during the voluntary contractions. The resulting extension in that direction is  $e$  ( $e > 0$ : elongation,  $e < 0$ : contraction). Then a simple analysis (Chadwick 1993) shows that  $\sigma_{11} = E_L e$ , as expected.

## 2.2. Third-order expansion of the strain energy in a TI incompressible solid

Acousto-elasticity calls for a third-order expansion of the elastic strain energy  $W$  in the powers of  $\mathbf{E}$ , the Green–Lagrange strain tensor. For TI incompressible solids, the expansion can be written as (Destrade *et al* 2010a)

$$W = \mu_T I_2 + \alpha_1 I_4^2 + \alpha_2 I_5 + \frac{A}{3} I_3 + \alpha_3 I_2 I_4 + \alpha_4 I_4^3 + \alpha_5 I_4 I_5, \quad (2)$$

where the second-order elastic constants  $\alpha_1, \alpha_2$  are given by

$$\alpha_1 = \frac{1}{2}(E_L + \mu_T - 4\mu_L), \quad \alpha_2 = 2(\mu_L - \mu_T), \quad (3)$$

and  $A, \alpha_3, \alpha_4$  and  $\alpha_5$  are third-order elastic constants. The strain invariants used in (2) are

$$I_2 = \text{tr}(\mathbf{E}^2), \quad I_3 = \text{tr}(\mathbf{E}^3), \quad I_4 = \mathbf{A} \cdot \mathbf{E} \mathbf{A}, \quad I_5 = \mathbf{A} \cdot \mathbf{E}^2 \mathbf{A}, \quad (4)$$

where  $\mathbf{A}$  is the unit vector in the fibres direction when the solid is unloaded and at rest. Note that Li and Cao (2020) call  $\alpha_1$  the  $C_{qsv}$  parameter, because it quantifies the spatial dependence of the speed  $v_{qsv}$  for the quasi shear vertical mode wave in an undeformed TI solid. Li and Cao (2020) show that  $\alpha_1$  can be negative or positive (with  $2\alpha_1 > -4\mu_L$ , because  $E_L + \mu_T > 0$ ).

For isotropic third-order elasticity, Gennisson *et al* (2007) measured the parameter  $A$  for soft phantom gels and found that it can be positive or negative even for solids which have a similar second-order shear modulus  $\mu$ . Hence they found  $\mu = 8.5$  kPa,  $A = -21.5$  kPa for a gelatin–agar phantom gel, and  $\mu = 8.1$  kPa,  $A = +10.7$  kPa for a PVA phantom gel. Thus there is an important difference from the nonlinear point of view between these two kinds of material even if their linear shear modulus are quite similar. As we will see, this remark carries over to TI muscle, where the hardening effect with effort proves to be much more important than the stiffness at rest.

## 2.3. Elastic waves in incompressible TI solids under uni-axial stress

We now study the propagation of small-amplitude plane body waves in a deformed, TI incompressible soft tissue. Destrade *et al* (2010a) or Ogden and Singh (2011) show that it is equivalent to solving a  $2 \times 2$  eigenproblem for the acoustical (symmetric) tensor. Its eigenvectors are orthogonal and give the two possible directions of transverse polarization; its eigenvalues are real and give the corresponding wave speeds.

One eigenvector is  $\mathbf{b} = \mathbf{A} \times \mathbf{n}$ , orthogonal to both the fibres and the direction of propagation  $\mathbf{n}$  (see figure 1). It corresponds to the shear-horizontal (SH) wave mode. The second one is  $\mathbf{a} = \mathbf{b} \times \mathbf{n}$  which lies in the shear-vertical (SV) plane. Calculations of their wave speed  $v$  as a function of the uni-axial stress  $\sigma_{11}$ , the propagation angle  $\theta$  and the second and third order elastic moduli are detailed in the supplementary file available online at [stacks.iop.org/PMB/66/145009/mmedia](https://stacks.iop.org/PMB/66/145009/mmedia). In our experiments, the radiation force  $\mathbf{F}$  used to induce the transient shear wave is applied along the  $x_3$  axis. Ultrasound tracking measures the  $x_3$  component of the shear wave displacement and is sensitive only to the (SH) propagation mode.

We may introduce the non-dimensional coefficients of nonlinearity  $\beta_{\parallel}$  and  $\beta_{\perp}$  as

$$\beta_{\parallel} = 1 + \frac{1}{E_L} \left( \mu_L - \mu_T + \frac{A}{4} + \alpha_3 + \frac{\alpha_5}{2} \right), \quad (5)$$

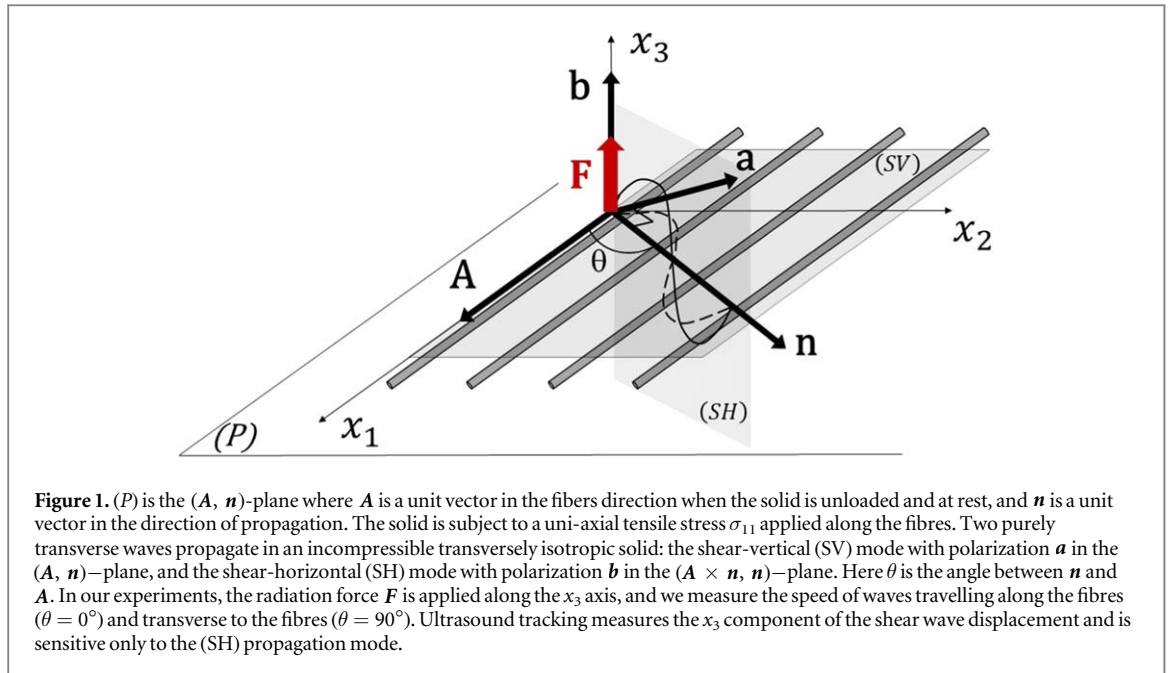
$$\beta_{\perp} = \frac{1}{E_L} \left( 3\mu_T + \frac{A}{2} - \alpha_3 \right), \quad (6)$$

to write see details in the supplementary material the acousto-elasticity equation of the (SH) mode as follows

$$\rho_0 v^2 = (\mu_L - \beta_{\parallel} \sigma_{11}) \cos^2 \theta + (\mu_T + \beta_{\perp} \sigma_{11}) \sin^2 \theta. \quad (7)$$

This equation takes into account the propagation angle  $\theta$  in the (SH) plane and is more general than relations obtained with a different approach by Bied *et al* (2020) for special cases  $\theta = 0^\circ$  (propagation *along the fibres*) and  $\theta = 90^\circ$  (propagation *transversely to the fibres*).

Here  $\rho_0$  is the mass density, which remains constant throughout the deformation because of incompressibility. In this paper, we take  $\rho_0 = 1000$  kg m<sup>-3</sup>, because most human soft tissues are assumed to have the same density as water. Notice that neither speed depends on the third-order constant  $\alpha_4$ , and that the speed of waves travelling transversely to the fibres does not depend on  $\mu_L$  and  $\alpha_5$  either. However, the



longitudinal Young modulus  $E_L$  does appear in that speed's expression, showing the interplay of axial and transverse linear parameters in the acousto-elastic effect.

### 3. Materials and methods

#### 3.1. Study purpose

Our goal is to measure the changes in the muscle stiffness, as measured by  $\rho v^2$  for the (SH) waves, as a function of the stress  $\sigma_{11}$  produced by a striated muscle during isometric contraction.

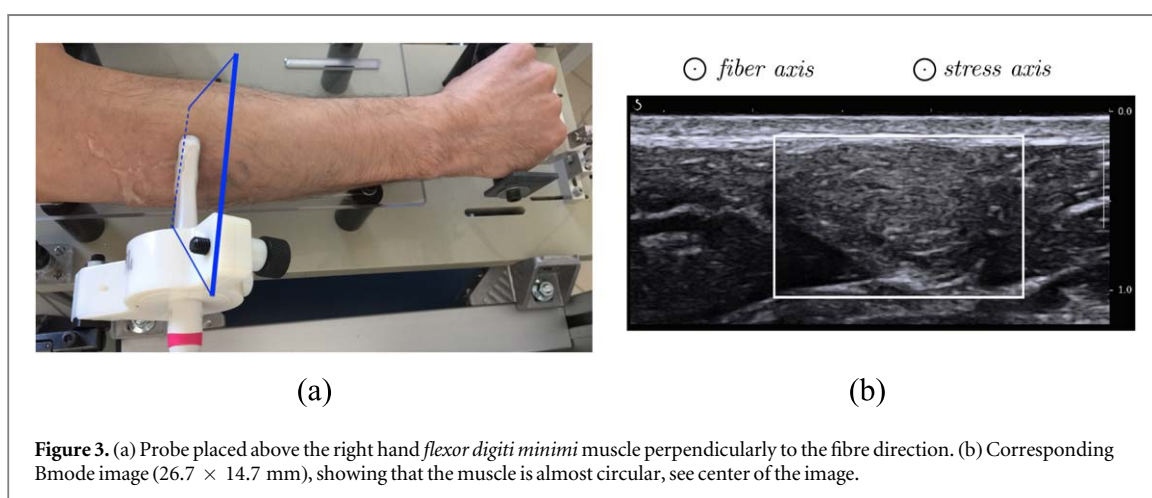
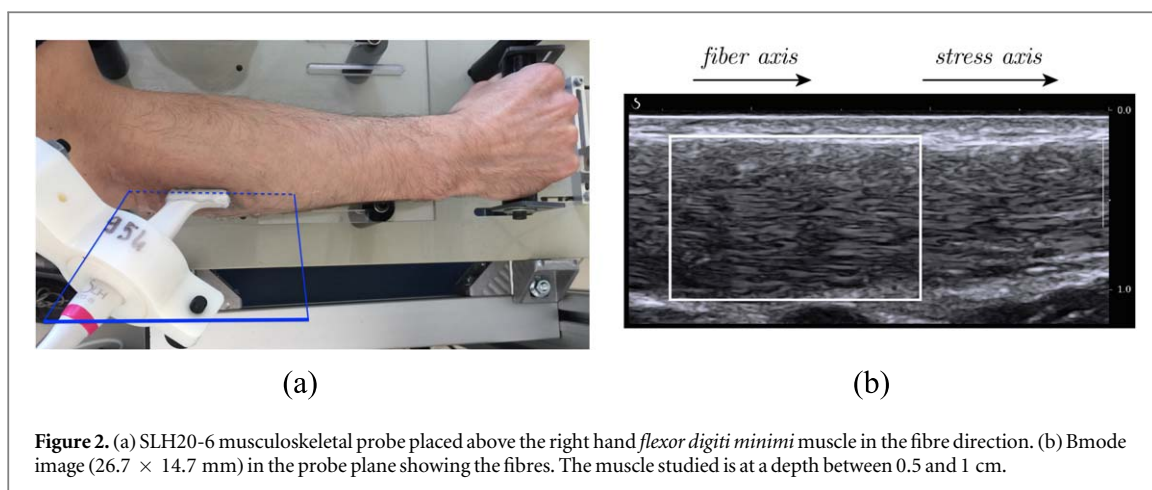
For this purpose, we use the SWE method, as provided by the Supersonic Shear Imaging technique included into the Aixplorer Imaging System (Supersonic Imagine, Aix en Provence, France, version V12.3). In principle, shear viscosity, which is frequency-dependent, is expected to modify the shear wave speed measured by the SWE technique. However, if the shear viscosity is small compared to the shear elastic modulus, the dispersion effect is limited and the muscle can be considered as a purely elastic medium. Moreover, as shown by Bercoff *et al* (2004), the effect of soft tissue viscosity on the shear wave speed is small provided the attenuation length is much larger than the wavelength. In our experiments, the S wave bandwidth at  $-6$  dB extends from 128 Hz to 1.28 kHz, i.e a 1.15 kHz bandwidth. The S wave central frequency is 704 Hz.

We call  $\mu = \rho_0 v^2$  the 'apparent shear modulus'. In our *in vivo* study, we measure the changes in  $\mu_{\parallel} = \mu_{\parallel}(\sigma_{11})$  along the fibre direction and the changes in  $\mu_{\perp} = \mu_{\perp}(\sigma_{11})$  transversely to the fibre direction, with the axial stress  $\sigma_{11}$  produced by the muscle. Then we use inverse analysis to link these experimental results to the acoustic-elasticity theory developed in section 2. We carry an *in vivo* feasibility study on six healthy volunteers with different age and sex.

#### 3.2. Muscle and imaging plane

The structure of muscles is complicated by inhomogeneities in fibre orientation and interfaces between fibre bundles. To isolate the behaviour of an individual muscle, unaffected by the complementary or antagonistic actions of other muscles, we select the *flexor digiti minimi* muscle, which extends the hand's little finger. This muscle is the only one involved in the little finger's extension, it has homogeneous fibre orientation (TI symmetry), and it is close to the epidermis, which matters for the relatively high frequency probe (SLH20-6 SSI probe, 12 MHz center frequency) used for the SWE measurements. Furthermore, as shown in figures 2–3, this muscle is convenient for probing, as it is situated on the side at the top of the forearm and spans over a distance longer than the 26.7 mm imaging width of the SLH20-6 probe.

We took particular care not to apply pressure with the probe on the skin surface because the tissue elasticity under the probe would be modified accordingly. Then, there would be two uni-axial forces: one induced by the voluntary contraction oriented along the  $x_1$  axis, and another caused by the probe pressure oriented vertically along the  $x_3$  axis and our equations would not apply. Thus the probe is just placed on the skin surface with ultrasound coupling gel. The probe is held by an articulated arm (H rger and G bler) which allows a 3D

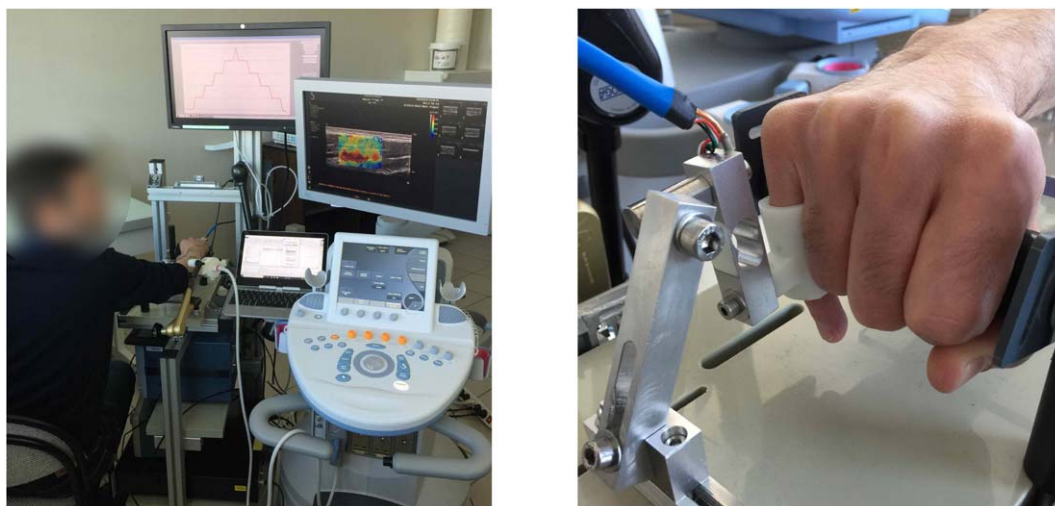


displacement of the probe for positioning and has a unique locking screw for quick lock-in (see figure 4(a)). We 3D printed a probe support that fits on this articulated arm. On figures 2(a) and 3(a) we can see the probe held axially and transversely to the fibre direction by this free arm which can be locked in the desired position.

The precise muscle localisation and the probe positioning are a difficult steps in the experimental preparation. The quality of the ultrasound imaging system and the choice of the ultrasound probe center frequency is particularly important since the *flexor digiti minimi* muscle has a diameter of about 0.6 cm. This positioning was realized by an experienced orthopedic surgeon who knows the anatomy of the upper limbs perfectly. One way to precisely localize the muscle on the image is to move slowly the little finger and look at the lateral tissue displacement in real time, with the probe positioned in the fibre direction. We chose to place the probe at the thickest part of the muscle which is located closer to the elbow than the wrist. This position is obtained when the lower interface of the *flexor digiti minimi* muscle is parallel to the probe (see figure 2(b) with the region of interest (ROI) inside the white box). When we move away from this position, the thickness of the muscle progressively decreases. We can see on the right of the figure 2(b) that the lower part of the muscle goes up on the image. The positioning in the axis of the fibers is optimized so that the echoes of the muscle fibers are as long as possible on the B mode image. These fibers are visible on the ultrasound B mode image by a slightly larger echo amplitude (see figure 2(b)). When the probe is perpendicular to the fiber's orientation, on the contrary, we are looking for the most punctual echoes possible of the muscle fibres and the smallest area of the muscle. As shown in figure 3(b) for a representative subject at rest, the perpendicular section of the right hand *flexor digiti minimi* muscle is clearly visible on the B mode image. The image dimension is 14.7 mm depth by 26.7 mm width, giving an idea of the small size of the muscle. The white boxes delimit the ROI, where SWE data are acquired.

### 3.3. Protocol and participants

Figure 4 shows the experimental setup including the custom-made force measurement system and the ultrasound imaging system.



(a) The subject is seated with their right elbow flexed at  $135^\circ$  ( $180^\circ$  corresponds to the full extension of the elbow) and positioned vertically at approximately  $70^\circ$  to the body.

(b) The little finger's first phalanx is placed vertically and in contact with a cylindrical rigid interface. The finger is aligned with the force sensor.

**Figure 4.** Experimental setup including the custom-made force measurement system and the US Aixplorer imaging system running the SonicLab V12 research software to upload the shear wave elastography (SWE) sequence.

**Table 1.** Age, sex, R/L handedness, maximum lifted load, maximum voluntary force, *flexor digiti minimi* muscle surface and maximum axial stress  $\sigma_{11\text{Max}}$  for the six healthy volunteers involved in the feasibility trial.

Subject	Age (years)	Sex (M/F)	Handedness R/L	Maximum load lifted (g)	Maximum voluntary force (N)	Muscle surface (cm <sup>2</sup> )	$\sigma_{11\text{Max}}$ (kPa)
#1	22	M	R	630	6.30	0.28	225
#2	62	M	R	725	7.25	0.27	268
#3	22	F	R	699	6.99	0.14	499
#4	25	F	R	525	5.25	0.2	262
#5	40	M	R	906	9.06	0.5	181
#6	32	M	R	902	9.02	0.55	164

Two women and four men, all right-handed, took part in this feasibility trial. They were informed of the possible risk and discomfort associated with the experimental procedures prior to giving their written consent to participate. Neither pregnant women nor persons under guardianship were included. The experimental design of this study was approved by the local Ethical Committee (Number ID RCB: 2020-A01601-38) and was carried out in accordance with the Declaration of Helsinki.

The subjects are seated with their right elbow flexed to  $135^\circ$  ( $180^\circ$  corresponds to the full extension of the elbow) and positioned vertically at approximately  $70^\circ$  to the body. The first phalanx of the little finger is placed vertically and in contact with a cylindrical rigid interface (figure 4(b)), so that it is aligned with the calibrated force sensor (micro load cell CZL635-20) and at rest. A lever arm, approximately 3 cm long, is placed between the force measuring point and the axis of rotation of the finger. That short distance might lead to a small difference between the magnitude of the force created inside the extensor muscle and the force measured by the sensor. At any rate, we assume that this effect is reflected by a small proportionality factor, which we neglect in our analysis. First, we asked the subjects to perform three maximum isometric voluntary contractions (MVC) lasting at least 3 s and separated by 30 s of recovery. The largest of the three forces was considered as the maximum voluntary force and was used to normalize subsequent submaximal contractions.

Table 1 details the age, sex, handedness, maximum voluntary force developed with the little finger, diameter of the muscle and finally, the maximum axial stress  $\sigma_{11\text{Max}}$  calculated by dividing the MVC force by the current muscle cross-surface area (obtained using the Bmode image in the direction transverse to the fibre direction). Interestingly, in spite of their great age difference (40 years), Subject#2 and Subject#3 (both male) develop the same maximum force magnitude (the maximum lifted load difference is only 26 g) but Subject#2 has twice the

muscle cross-surface area as Subject#3. Thus the maximum voluntary stress  $\sigma_{11\text{Max}}$  induced by Subject#2 is half that of Subject#3. On the other hand, the axial stress  $\sigma_{11\text{Max}}$  obtained by Subject#5 is one of the smallest in the cohort, while its maximum lifted load is the largest. We also note that the maximum voluntary force range is large, from a low of 5.25 N for Subject#4 to a high of 9.06 N for Subject#5.

Then the participants were asked to perform five voluntary contractions at levels corresponding to 4%, 8%, 12%, 16%, 20% of MVC. They had to stay 4 s at each stage before moving to the next level. This period provided sufficient time to save the SWE image on the Aixplorer (and to allow for some viscous dissipation). To control the force steps, the participants followed a visual feedback displayed on a monitor placed in front of them, see figure 4(a). It turned out to be difficult for some subjects to maintain precisely a constant force, especially at the 16% and 20% levels of the MVC. For this reason we conducted our inverse analysis for measurements up to 12% only, see results in section 4.

### 3.4. SWE measurements

We used the SWE method to measure how shear elasticity changed with the force applied by the volunteers during the isometric contraction protocol.

The SWE experiment is based on two steps: the generation of the shear waves and the ultrafast imaging of their propagation. In our experiments, the central frequency of the fast imaging scheme is 7.5 MHz and the image repetition frequency is set to 14 kHz, adapted to muscle stiffness.

For the B mode image, the lateral distance is linked to the SLH20-6 probe number of elements and pitch (140  $\mu\text{m}$ ) and is equal to 26.7 mm (see legends in figures 2 or 3). The maximum axial distance is selected as desired and is 14.7 mm in figures 2(b) and 3(b). For SWE acquisition, we select a ROI delimited with the white rectangle on the figures 2(b) and 3(b). Thus the region where the SWE data are recorded is a smaller region than the complete B mode image. This region where the elasticity is measured is also visible on figures 6 and 9. We can modify the shape and the surface of this rectangle to fit the ROI containing the muscle.

On the SWE grid, there are 44 sampling points along the vertical axis, between the depths of 2.3 and 11.2 mm, with an axial resolution corresponding to one ultrasonic wavelength at 7.5 MHz, i.e 205  $\mu\text{m}$ . There are 110 sampling points along the lateral axis, between 1.5 and 16.8 mm, with the lateral resolution of SLH20-6 probe pitch. On figures 5 and 8, spatial data are referenced in the SWE grid and the first pixel at position (0 mm, 0 mm) is located at the top left of the images. This pixel correspond to the pixel situated at (2.3 mm, 1.5 mm) in the Bmode image. The last pixel is located at the bottom right of the images at the position (8.9 mm, 15.3 mm) and corresponds to the pixel (11.2 mm, 16.8 mm) in the Bmode image grid.

An SWE acquisition consists of five pushing lines positioned laterally at  $-0.23, 3.77, 7.77, 11.77, 15.77$  mm in the SWE grid.

There are 48 frames in the temporal dimension, with a spatial resolution of 71.4  $\mu\text{s}$ . Hence, we record the SW propagation for 3.4 ms, which is sufficient to follow the wave propagating along the width of the probe. The time  $t = 0$  ms in figure 5 correspond to the beginning of the SWE data acquisition which is situated after the beginning of the push sequence.

## 4. Results

### 4.1. Propagation along the fibres

Figure 5 shows the shear wave propagation induced in the muscle by the ultrasonic transient radiation force for Subject#5 at rest. The radiation force is applied vertically along the positive  $x_3$  axis. The wave propagates in the fibre direction along the  $x_1$  axis and is polarized along the  $x_3$  axis. The propagation is presented at four different times:  $t = 0, 0.21, 0.43, 0.64$  ms, with a color scheme for the tissue particle velocity, superimposed onto the Bmode image. The color scale is adapted for each image to take into account wave attenuation and enhance visualization. Note that here the Bmode image is obtained from the shear wave tracking sequence and has a lower quality than the Bmode image shown in figure 2. For this figure, we selected the third push zone situated at the lateral position 7.77 mm in the SWE grid.

At time  $t = 0.64$  ms, we can clearly see that the lower part of the shear wave front is ahead of the other parts of the wave front, indicating that the wave propagates faster in the muscle. Thus, we select the ROI in that lower part of the muscle for the measurements with the diagnostic mode of the Aixplorer. In this region, the muscle tissue is homogeneous since the shear wave front remains vertical during propagation.

We assume that the phase speed dispersion is small at that the SWE measurement gives the speed of all shear waves with different frequencies in the wave packet. Further, we assume that viscosity might attenuate the amplitude of the wave, but does not modify its speed noticeably (Bercoff et al 2004).

Figures 6 show the measurements given by the SWE diagnostic mode of the Aixplorer, obtained for Subject#5 at four levels of voluntary contraction: 0%, 4%, 8%, 12% of MVC, corresponding to  $\sigma_{11}$  equal to 0,

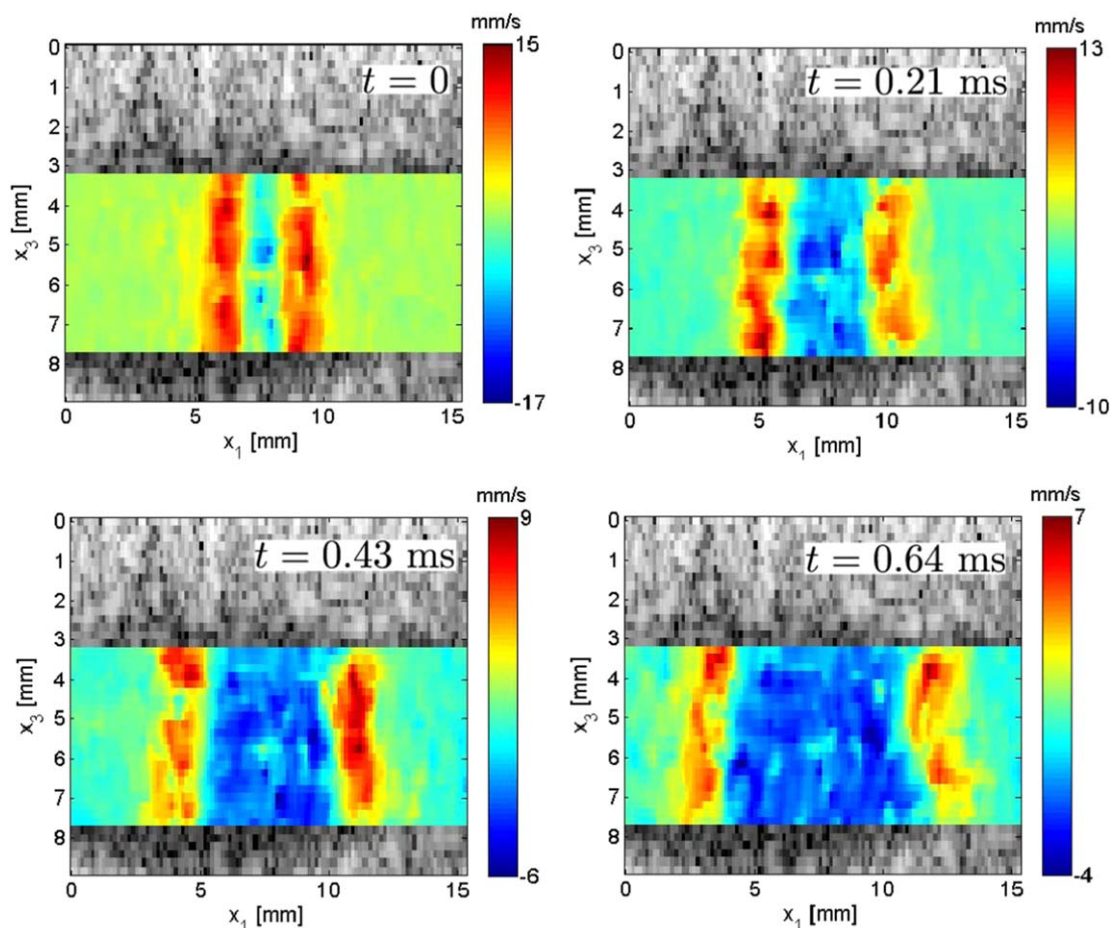


Figure 5. Shear wave (SH mode) propagation along the *flexor digiti minimi* muscle fibres for Subject#5 at rest. The wave propagates in the fibres direction  $x_1$  and is polarized vertically along the  $x_3$  axis. The color gives the tissue particle velocity at each location, see scale on the right (which adapts for better visualization).

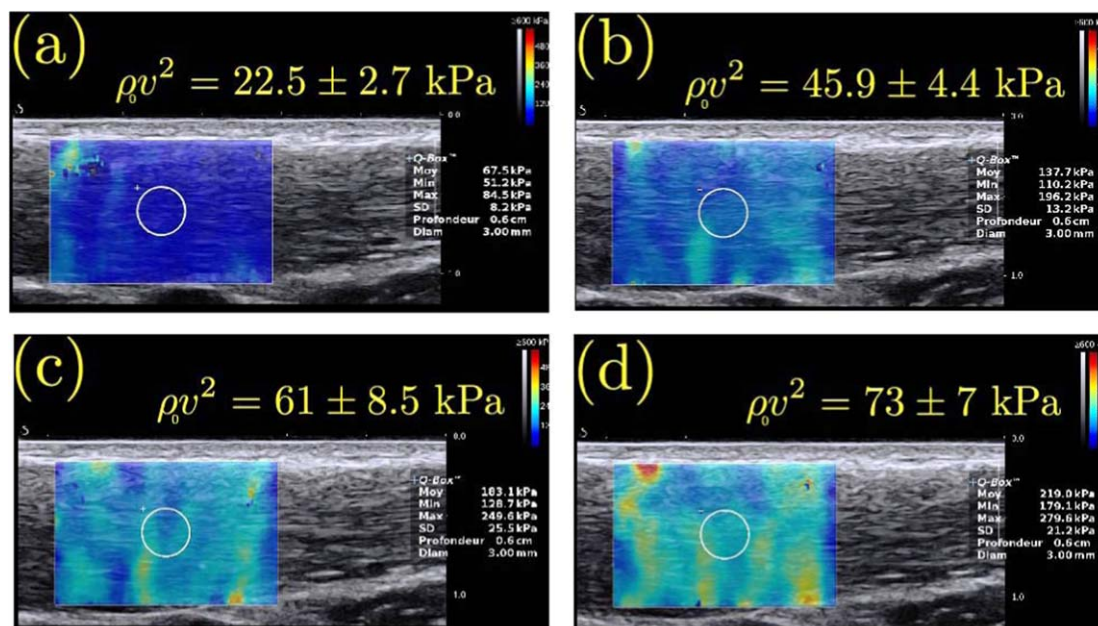
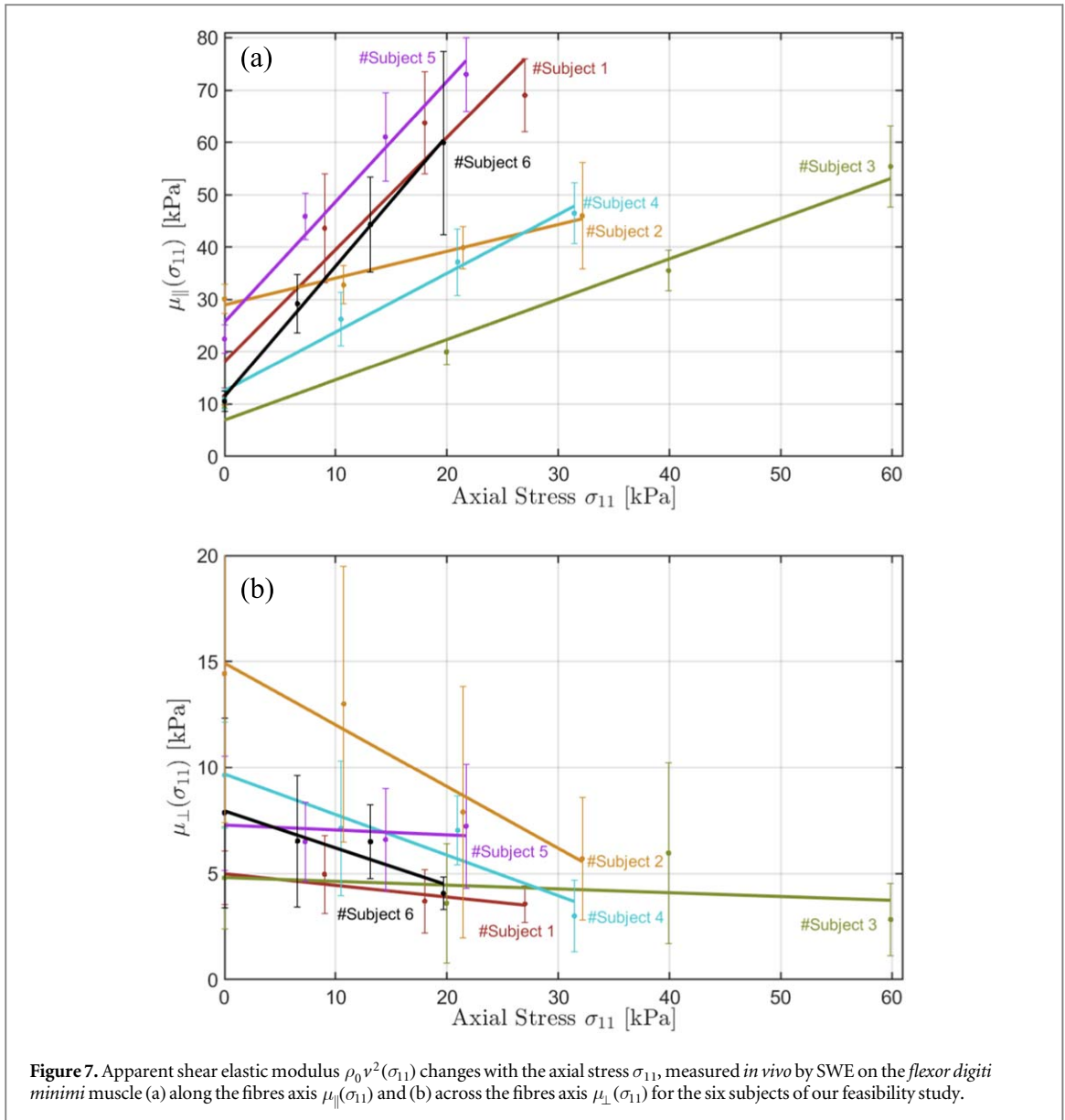


Figure 6. SWE analysis for Subject#5 at four levels of voluntary contraction along the *flexor digiti minimi* muscle fibres. (a): At rest, (b): 4% MVC, (c): 8% MVC, (d): 12% MVC. From the Aixplorer measure we deduce the average wave speed in the ROI (disc inside white circle) and compute the apparent axial shear modulus  $\mu_{||}(\sigma_{11}) = \rho_0 v^2$ . For this subject, it increases with the applied stress.



7.2, 14.5, and 21.7 kPa, respectively. The machine gives a ‘stiffness’ value, obtained by multiplying  $\rho_0 v^2$  by 3 to yield the apparent isotropic Young modulus. However here the material is anisotropic and we cannot use that formula. Instead we simply divide back the machine mean value over the selected ROI (say  $67.5 \pm 8.2$  kPa at rest, figure 6(a)) by 3 (to obtain  $\rho_0 v^2 = 22.5 \pm 2.7$  kPa at rest, for example).

We collected the measurements on figure 7(a) for the six volunteers. We notice a linear variation of  $\mu_{\parallel}(\sigma_{11})$  with  $\sigma_{11}$  in the fibres direction, similar to the behaviour obtained experimentally by Bouillard *et al* (2011) on the *abductor digiti minimi* muscle. This variation is also in line with our theoretical analysis, according to which  $\mu_{\parallel}(\sigma_{11}) = \rho_0 v^2$  is given by (7) with  $\theta = 0$  as

$$\mu_{\parallel}(\sigma_{11}) = \mu_L - \beta_{\parallel} \sigma_{11}, \quad (8)$$

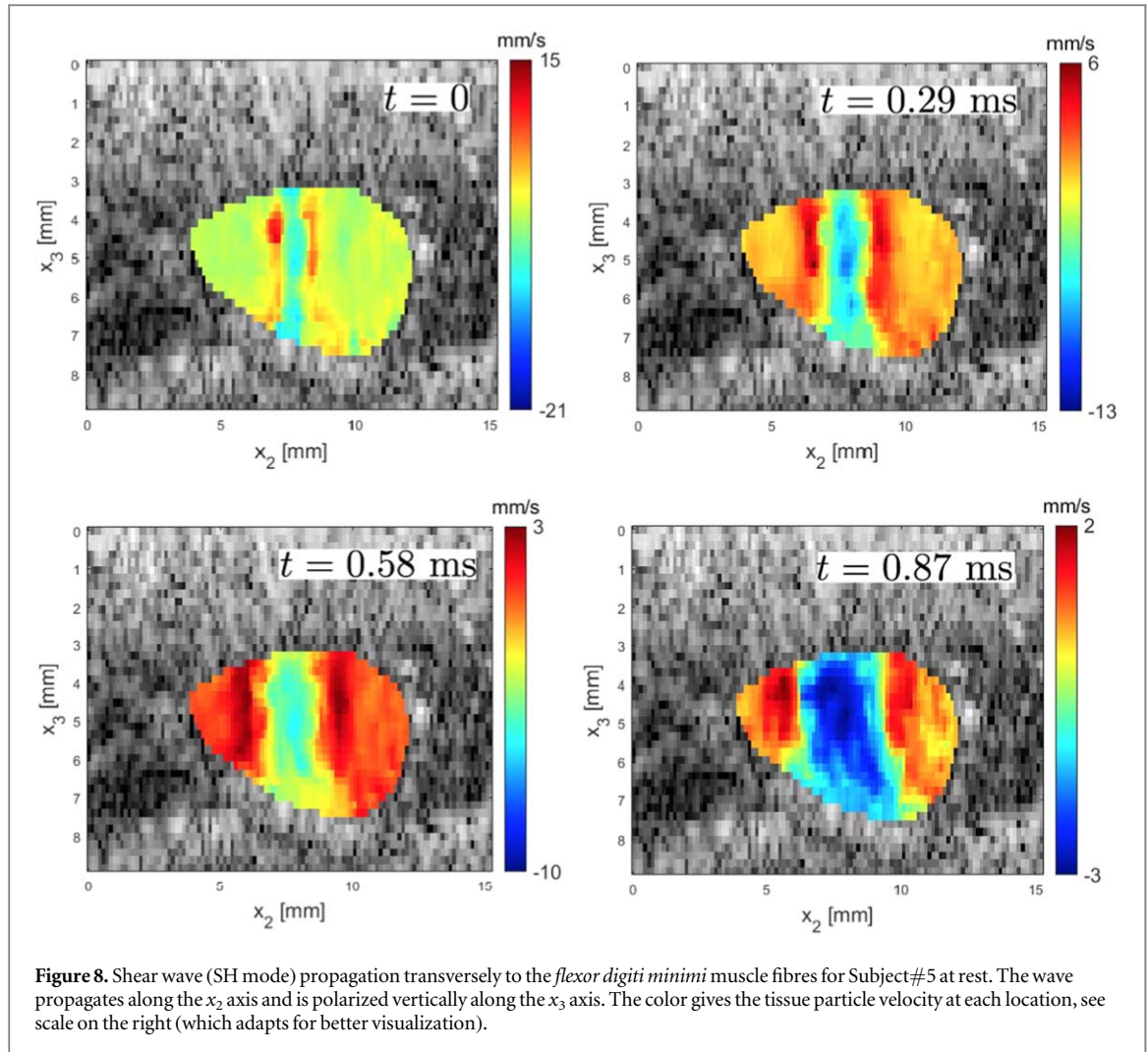
where the non-dimensional coefficient of nonlinearity  $\beta_{\parallel}$  is given by (5).

For all six subjects,  $\mu_{\parallel}(\sigma_{11})$  increases with  $\sigma_{11}$ , so that  $\beta_{\parallel} < 0$  in the cohort.

For the curve-fitting exercise determining the quantities  $\mu_L$  and  $\beta_{\parallel}$ , we use the Matlab *robustfit* algorithm which allocates lower weight to points that do not fit well. It also outputs the coefficient of determination  $R^2$  and the root mean squared error  $RMS_e$ .

#### 4.2. Propagation across the fibres

In the direction transverse to the muscle fibres, the shear wave is highly scattered by heterogeneities, which induces a poor signal-to-noise ratio for frequency analysis (Defieux *et al* 2008b).



Figures 8 show the shear wave propagation perpendicularly to the fibres axis for Subject #5, at four different times:  $t = 0, 0.29, 0.58, 0.87$  ms. Superimposed onto the Bmode image, we show the propagation inside the muscle only, which has a quasi-circular shape with a diameter of approximately 8 mm (see figure 3 for a more precise localisation of the muscle with a better Bmode image quality).

Figures 9 show the values of the apparent shear modulus  $\mu_{\perp}(\sigma_{11}) = \rho_0 v^2$  in the transverse direction, for Subject #5. Again, we present measurements up to 12% of MVC.

According to our theoretical analysis,  $\mu_{\perp}(\sigma_{11})$  is equal to  $\rho_0 v^2$  given by (7) with  $\theta = 90^\circ$  as

$$\mu_{\perp}(\sigma_{11}) = \mu_T + \beta_{\perp} \sigma_{11}, \quad (9)$$

where the non-dimensional coefficient of nonlinearity  $\beta_{\perp}$  is given by (6).

Again, we use the formula from acoustic-elasticity theory to produce a linear fit to the data. In contrast to the case of propagation along the fibres, we find that  $\mu_{\perp}(\sigma_{11})$  does not increase with the axial stress  $\sigma_{11}$ , but decreases slightly for Subject #5. Other subjects lead to different behaviours, as can be checked on figure 7(b), but  $\beta_{\perp}$  is always negative in the cohort. We summarise the results in table 2.

## 5. Discussion

Using acousto-elasticity theory, we obtained analytical expressions for the dependence of the SH shear wave speed as a function of the applied uniaxial stress in muscle, assuming that it behaves as a TI, incompressible soft solid, and that the wave travels either along or transverse to the fibres.

For our experiments, we oriented the acoustic radiation force along the vertical axis and propagated the wave along or transverse to the *flexor digiti minimi* muscle to avoid coupling of the SH mode with the SV mode (Rouze et al 2020). We determined theoretically and experimentally the apparent shear elastic modulus  $\mu(\sigma_{11}) = \rho_0 v^2$ , and found it varies linearly with  $\sigma_{11}$ .

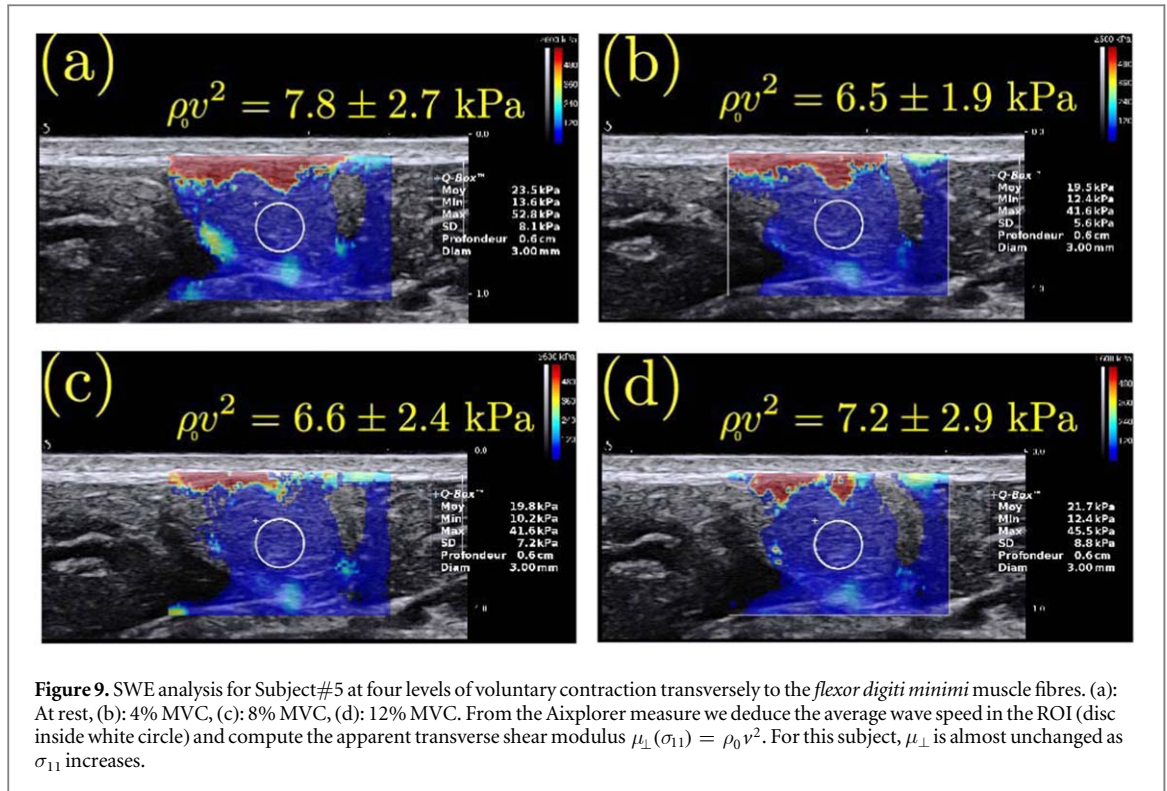


**Table 2.** Axial shear elastic modulus at rest  $\mu_L$ , axial nonlinearity coefficient  $\beta_{\parallel}$ , transverse shear elastic modulus at rest  $\mu_T$ , transverse nonlinearity parameter  $\beta_{\perp}$ , 12% of maximum axial stress  $\sigma_{11\text{Max}}$  for the *flexor digiti minimi* muscle of the six healthy volunteers involved in the study.

Subject	$\mu_L$ (kPa)	$\beta_{\parallel}$	$R^2$	$\mu_T$ (kPa)	$\beta_{\perp}$	$R^2$	$0.12\sigma_{11\text{Max}}$ (kPa)
#1	$18.1 \pm 8.9$	$-2.14 \pm 0.53$	0.89	$5.0 \pm 0.4$	$-0.05 \pm 0.02$	0.72	27.0
#2	$29.0 \pm 1.3$	$-0.51 \pm 0.07$	0.97	$14.9 \pm 1.0$	$-0.29 \pm 0.05$	0.94	32.2
#3	$6.9 \pm 3.0$	$-0.77 \pm 0.08$	0.98	$4.8 \pm 1.5$	$-0.02 \pm 0.04$	0.09	59.9
#4	$12.6 \pm 2.1$	$-1.12 \pm 0.10$	0.98	$9.7 \pm 1.0$	$-0.19 \pm 0.05$	0.87	31.4
#5	$25.7 \pm 3.9$	$-2.30 \pm 0.30$	0.96	$7.3 \pm 0.7$	$-0.02 \pm 0.05$	0.09	21.7
#6	$11.5 \pm 1.2$	$-2.50 \pm 0.09$	0.99	$7.9 \pm 0.6$	$-0.17 \pm 0.05$	0.85	19.7

We obtained analytical expressions for  $\mu_{\parallel}(\sigma_{11}) = \mu_L - \beta_{\parallel}\sigma_{11}$  in the fibre direction and for  $\mu_{\perp}(\sigma_{11}) = \mu_T + \beta_{\perp}\sigma_{11}$  transversely to the fibre direction. The coefficient  $\beta_{\parallel}$  is a linear combination of the second-order elastic parameters  $\mu_L, \mu_T, E_L$ , and the third-order moduli  $A, \alpha_3, \alpha_5$ ; the coefficient  $\beta_{\perp}$  is written in terms of only two second-order parameters  $\mu_T, E_L$  and two third-order moduli  $A, \alpha_3$ . Neither coefficient involves the other third-order parameter  $\alpha_4$ .

Our *in vivo* analysis of the six-volunteer cohort focused on the variation of the apparent shear elastic moduli with  $\sigma_{11}$ . The results show that these variations are very different across the cohort.

For the analysis of  $\mu_{\perp}(\sigma_{11})$ , we distinguish three subgroups.

For Subjects #2,4,6 (first group), we find  $\beta_{\perp} = -0.29, -0.19, -0.17 (\pm 0.05)$ , respectively, all negative, indicating that  $\mu_{\perp}$  decreases with  $\sigma_{11}$ . Here the connective tissue surrounding the muscle fibres softened under axial stress  $\sigma_{11}$ .

For Subjects #1,3,5, we find  $\beta_{\perp} = -0.05 \pm 0.02, -0.02 \pm 0.04, -0.02 \pm 0.05$ , respectively, all small values, indicating that  $\mu_{\perp}$  is almost unchanged as  $\sigma_{11}$  increases. For these three subjects, the infinitesimal shear elastic moduli  $\mu_T$  are almost the same:  $\mu_T = 5.0 \pm 0.4, 4.8 \pm 1.5, 7.3 \pm 0.7$  kPa, respectively. However, Subject #3 has a much greater value of 12% of maximum axial stress ( $12\% \sigma_{11\text{Max}} = 59.9$  kPa) than Subjects #1,5, who have approximately the same value (27.0, 21.7 kPa, respectively). Subject #3 also has a much lower magnitude of coefficient  $\beta_{\parallel}$  ( $= -0.77 \pm 0.08$ ) than Subjects #1,5 who have approximately the same  $\beta_{\parallel}$  coefficient ( $= -2.14 \pm 0.53, -2.3 \pm 0.30$ ). Thus, we separate Subjects #1,5 (second group) from Subject #3 (third group).

By comparing expressions (5) and (6) for the  $\beta$  nonlinearity coefficients, we see that only the  $\mu_{\perp}$  and  $\alpha_5$  parameters can explain why  $\beta_{\parallel}$  is different between the second and the third group, because they do not appear in the expression (6) for  $\beta_{\perp}$  (which is the same for these two groups). Hence we see that a higher value of  $\mu_{\perp}$  in (5) results in a higher value of the coefficient  $\beta_{\parallel}$  for subjects who have an identical  $\beta_{\perp}$ . This is indeed what we observed experimentally, see values in table 2.

For the analysis of the axial apparent shear modulus  $\mu_{\parallel}(\sigma_{11})$ , we also find three subgroups, according to the magnitude of the nonlinearity coefficient  $\beta_{\parallel}$ . Hence Subjects#2,3 both present small magnitudes for  $\beta_{\parallel}$ , Subject#4 present intermediate value, and Subjects#1,5,6 all present high values (in that order).

For a contraction from rest to 12% MVC, Subject#6's apparent elastic modulus  $\mu_{\parallel}(\sigma_{11})$  increases by a factor 6, from 10.5 to 59.9 kPa, demonstrating his remarkable ability to recruit fibres to harden the muscle very quickly. On the *peroneus longus* muscle of anaesthetised cats, Petit *et al* (1990) found that the S motor units can produce high values of muscle stiffness, suggesting that for Subject#6, the motor units ratio S/F might be very high. Subject#6 also develops the smallest 12% of maximum axial stress value of the cohort, consistent with a high S/F ratio because slow (S) motor units develop quite small tensions compared with FR and FF units (Petit *et al* 1990).

For Subjects#1,5,6 (third group), we note that the higher the  $\beta_{\parallel}$  magnitude is ( $-2.41 \pm 0.53$ ,  $-2.3 \pm 0.30$ ,  $-2.5 \pm 0.09$ , respectively), the lower the maximal axial stress is  $\sigma_{11\text{Max}}$  (27.0 kPa, 21.7 kPa, 19.7 kPa, respectively).

For Subjects#2,3 (first group), we recorded the smallest magnitude of the nonlinearity coefficient  $\beta_{\parallel}$  ( $-0.51 \pm 0.07$ ,  $-0.77 \pm 0.08$ , respectively). These two subjects develop respectively the second-highest (32.2 kPa) and the highest (59.9 kPa) maximum axial stress 12%  $\sigma_{11\text{Max}}$  in the cohort. These results are consistent with a high presence of fast fibres (F) that do not harden rapidly the muscle, associated with a quite high tension Petit *et al* (1990).

A natural follow-up on this study is to apply the method to patients with musculoskeletal disorders or neurodegenerative diseases. However, the method must be adapted because we found it was difficult for some healthy subjects to maintain a voluntary constant force during the time required to measure the wave speed, a task which could prove even more challenging for patients. This adaptation could be achieved with a muscle contained hardening method, based on the corresponding nerve electro-stimulation associated with a synchronous measurement of force and elasticity. That set up would provide a calibrated and repeatable stimulation protocol as used for EMG measurements. A better localisation of the muscle and a better probe positioning in relation to the fibres orientation could be achieved by linking in real time the ultrasound Bmode image with the corresponding slice plan of a pre-acquired MRI volume image. The effect of the distance between the force sensor and the muscle could also be quantified precisely.

Finally, the modelling can be improved, to include heterogeneity, viscosity, dispersion, and an active stress contribution to the constitutive formulation.

## 6. Conclusion

The quantification of the elastic nonlinearity of biological tissues can prove to be a most valuable tool for the early diagnosis of musculoskeletal disorders. Here, we developed an acousto-elasticity theory to study the propagation of small-amplitude plane body waves in deformed TI incompressible solids. For the SH mode, we obtained a linear relation between the squared wave speed  $\rho_0 v^2$  and the applied axial stress  $\sigma_{11}$  using the second- and third-order elastic constants. Then we used this theory to analyse experimental results on skeletal striated muscle.

With a cohort of six healthy volunteers, we uncovered a great diversity for the nonlinear behaviour of the *flexor digiti minimi* muscle, for the apparent shear modulus  $\mu_{\parallel}(\sigma_{11})$  along the fibres as well as for the transverse apparent shear modulus  $\mu_{\perp}(\sigma_{11})$ . Hence  $\mu_{\perp}$  can decrease with  $\sigma_{11}$  (Subjects#2,4,6) or remain almost constant (Subjects#1,3,5). Meanwhile,  $\mu_{\parallel}$  always increases with  $\sigma_{11}$ , and the rate of increase is highly correlated to the weakness of the MVC produced by the volunteer.

## Acknowledgments

The author's have confirmed that any identifiable participants in this study have given their consent for publication. We thank V ronique Marchand-Pauvert (Laboratoire d'Imagerie Biom dicale, Sorbonne Universit ) for helpful discussions about the role of motor units in muscle function and their relationship to muscle elasticity. We also thank Jean-Marc Gregoire and Jean-Yves Tartu (iBrain Laboratory, Universit  de

Tours) for the development of the electronics and the mechanics of the force measurement device, respectively. This work is supported by the Institut du Biom dicament and by the INCA Plan Cancer BPALP project.

## ORCID iDs

Jean-Pierre Remeni ras  <https://orcid.org/0000-0001-8440-5184>

Jean-Luc Gennisson  <https://orcid.org/0000-0001-8318-8237>

Michel Destrade  <https://orcid.org/0000-0002-6266-1221>

## References

- Adams P F, Hendershot G E and Marano M A 1999 Current estimates from the National Health Interview Survey, 1996 *Vital Health Stat* **10** 1–203
- Badley E M, Rasooly I and Webster G K 1994 Relative importance of musculoskeletal disorders as a cause of chronic health problems, disability, and health care utilization: findings from the 1990 Ontario Health Survey *J. Rheumatol.* **21** 505–14
- Bayat M, Adabi S, Kumar V, Gregory A, Webb J, Denis M, Kim B, Singh A, Mynderse L and Husmann D 2019 Acoustoelasticity analysis of transient waves for non-invasive *in vivo* assessment of urinary bladder *Sci. Rep.* **9** 1–9
- Bercoff J, Tanter M, Muller M and Fink M 2004 The role of viscosity in the impulse diffraction field of elastic waves induced by the acoustic radiation force *IEEE Trans. Ultrason. Ferroelectr. Freq. Control* **51** 1523–36
- Bernal M, Chamming's F, Couade M, Bercoff J, Tanter M and Gennisson J-L 2015 *In vivo* quantification of the nonlinear shear modulus in breast lesions: feasibility study *IEEE Trans. Ultrason. Ferroelectr. Freq. Control* **63** 101–9
- Bied M, Jourdain L and Gennisson J-L 2020 Acoustoelasticity in transverse isotropic soft tissues: quantification of muscles' nonlinear elasticity *2020 IEEE Int. Ultrasonics Symp. (IUS) (Las Vegas, NV, 7–11 September 2020)* (Piscataway, NJ: IEEE) pp 1–4
- Bouillard K, Nordez A and Hug F 2011 Estimation of individual muscle force using elastography *PLoS One* **6** e29261
- Bouillard K, Jubeau M, Nordez A and Hug F 2014 Effect of vastus lateralis fatigue on load sharing between quadriceps femoris muscles during isometric knee extensions *J. Neurophysiol.* **111** 768–76
- Chadwick P 1993 Wave propagation in incompressible transversely isotropic elastic media I. Homogeneous plane waves *Proc. of the Royal Irish Academy* vol 93A (Royal Irish Academy) pp 231–53 <http://www.jstor.org/stable/20489459>
- Deffieux T, Gennisson J-L, Tanter M and Fink M 2008a Assessment of the mechanical properties of the musculoskeletal system using 2-D and 3-D very high frame rate ultrasound *IEEE Trans. Ultrason. Ferroelectr. Freq. Control* **55** 2177–90
- Deffieux T, Montaldo G, Tanter M and Fink M 2008b Shear wave spectroscopy for *in vivo* quantification of human soft tissues visco-elasticity *IEEE Trans. Med. Imaging* **28** 313–22
- Destrade M, Gilchrist M D and Ogden R W 2010a Third- and fourth-order elasticities of biological soft tissues *J. Acoust. Soc. Am.* **127** 2103–6
- Destrade M, Gilchrist M D and Saccomandi G 2010b Third- and fourth-order constants of incompressible soft solids and the acousto-elastic effect *J. Acoust. Soc. Am.* **127** 2759–63
- Dh'ooze J, Heimdal A, Jamal F, Kukulski T, Bijmens B, Rademakers F, Hatle L, Suetens P and Sutherland G R 2000 Regional strain and strain rate measurements by cardiac ultrasound: Principles, implementation and limitations *Eur. J. Echocardiogr.* **1** 154–70
- Downs M E, Lee S A, Yang G, Kim S, Wang Q and Konofagou E E 2018 Non-invasive peripheral nerve stimulation via focused ultrasound *in vivo Phys. Med. Biol.* **63** 035011
- Eranki A, Cortes N, Feren ek Z G and Sikdar S 2013 A novel application of musculoskeletal ultrasound imaging *J. Vis. Exp.* **79** e50595
- Ford L, Huxley A and Simmons R 1981 The relation between stiffness and filament overlap in stimulated frog muscle fibres *J. Physiol.* **311** 219–49
- Gennisson J-L, Catheline S, Chaffai S and Fink M 2003 Transient elastography in anisotropic medium: Application to the measurement of slow and fast shear wave speeds in muscles *J. Acoust. Soc. Am.* **114** 536–41
- Gennisson J-L, R n er M, Catheline S, Barri re C, Bercoff J, Tanter M and Fink M 2007 Acoustoelasticity in soft solids: assessment of the nonlinear shear modulus with the acoustic radiation force *J. Acoust. Soc. Am.* **122** 3211–9
- Gennisson J-L, Deffieux T, Mac e E, Montaldo G, Fink M and Tanter M 2010 Viscoelastic and anisotropic mechanical properties of *in vivo* muscle tissue assessed by supersonic shear imaging *Ultrasound Med. Biol.* **36** 789–801
- Gijsbertse K, Gosselink R, Lassche S, Nillesen M, Sprengers A, Verdonschot N, van Alfen N and De Korte C 2017 Ultrasound imaging of muscle contraction of the tibialis anterior in patients with facioscapulohumeral dystrophy *Ultrasound Med. Biol.* **43** 2537–45
- Hug F, Tucker K, Gennisson J-L, Tanter M and Nordez A 2015 Elastography for muscle biomechanics: Toward the estimation of individual muscle force *Exercise Sport Sci. Rev.* **43** 125–33
- Jacobson L, Lindgren B and Sjukdomarna V 1996 What are the costs of illness? *Stockholm: Socialstyrelsen* (Sweden: National Board of Health and Welfare)
- Jiang Y, Li G, Qian L-X, Liang S, Destrade M and Cao Y 2015 Measuring the linear and nonlinear elastic properties of brain tissue with shear waves and inverse analysis *Biomech. Model. Mechanobiol.* **14** 1119–28
- Kim K, Hwang H-J, Kim S-G, Lee J-H and Jeong W K 2018 Can shoulder muscle activity be evaluated with ultrasound shear wave elastography? *Clin. Orthop. Relat. Res.* **476** 1276–83
- Koo T K, Guo J-Y, Cohen J H and Parker K J 2014 Quantifying the passive stretching response of human tibialis anterior muscle using shear wave elastography *Clin. Biomech.* **29** 33–9
- Latorre-Ossa H, Gennisson J-L, De Broesses E and Tanter M 2012 Quantitative imaging of nonlinear shear modulus by combining static elastography and shear wave elastography *IEEE Trans. Ultrason. Ferroelectr. Freq. Control* **59** 833–9
- Li G-Y and Cao Y 2020 Backward Mach cone of shear waves induced by a moving force in soft anisotropic materials *J. Mech. Phys. Solids* **138** 103896
- Li G-Y, Zheng Y, Liu Y, Destrade M and Cao Y 2016 Elastic Cherenkov effects in transversely isotropic soft materials-i: theoretical analysis, simulations and inverse method *J. Mech. Phys. Solids* **96** 388–410
- Lopata R G, van Dijk J P, Pillen S, Nillesen M M, Maas H, Thijssen J M, Stegeman D F and de Korte C L 2010 Dynamic imaging of skeletal muscle contraction in three orthogonal directions *J. Appl. Physiol.* **109** 906–15
- Loram I D, Maganaris C N and L kie M 2006 Use of ultrasound to make noninvasive *in vivo* measurement of continuous changes in human muscle contractile length *J. Appl. Physiol.* **100** 1311–23

- Miyatake K, Yamagishi M, Tanaka N, Uematsu M, Yamazaki N, Mine Y, Sano A and Hirama M 1995 New method for evaluating left ventricular wall motion by color-coded tissue doppler imaging: *in vitro* and *in vivo* studies *J. Am. College Cardiol.* **25** 717–24
- Nagueh S F, Mikati I, Kopelen H A, Middleton K J, Qui ones M A and Zoghbi W A 1998 Doppler estimation of left ventricular filling pressure in sinus tachycardia: a new application of tissue doppler imaging *Circulation* **98** 1644–50
- Nordez A and Hug F 2010 Muscle shear elastic modulus measured using supersonic shear imaging is highly related to muscle activity level *J. Appl. Physiol.* **108** 1389–94
- Nordez A, Genisson J L, Casari P, Catheline S and Cornu C 2008 Characterization of muscle belly elastic properties during passive stretching using transient elastography *J. Biomech.* **41** 2305–11
- Ogden R W and Singh B 2011 Propagation of waves in an incompressible transversely isotropic elastic solid with initial stress: Biot revisited *J. Mech. Mater. Struct.* **6** 453–77
- Otesteanu C F, Chintada B R, Rominger M B, Sanabria S J and Goksel O 2019 Spectral quantification of nonlinear elasticity using acoustoelasticity and shear-wave dispersion *IEEE Trans. Ultrason. Ferroelectr. Freq. Control* **66** 1845–55
- Papazoglou S, Rump J, Braun J and Sack I 2006 Shear wave group velocity inversion in mr elastography of human skeletal muscle *Magn. Reson. Med.* **56** 489–97
- Petit J, Filippi G, Emonet-Denand F, Hunt C and Laporte Y 1990 Changes in muscle stiffness produced by motor units of different types in peroneus longus muscle of cat *J. Neurophysiol.* **63** 190–7
- Reginster J-Y and Khaltayev N 2002 Introduction and WHO perspective on the global burden of musculoskeletal conditions *Rheumatology* **41** 1–2
- Rouze N C, Wang M H, Palmeri M L and Nightingale K R 2013 Finite element modeling of impulsive excitation and shear wave propagation in an incompressible, transversely isotropic medium *J. Biomech.* **46** 2761–8
- Rouze N C, Palmeri M L and Nightingale K R 2020 Tractable calculation of the Green’s tensor for shear wave propagation in an incompressible, transversely isotropic material *Phys. Med. Biol.* **65** 015014
- Sarvazyan A P, Rudenko O V, Swanson S D, Fowlkes J B and Emelianov S Y 1998 Shear wave elasticity imaging: a new ultrasonic technology of medical diagnostics *Ultrasound Med. Biol.* **24** 1419–35
- Storheim K and Zwart J-A 2014 Musculoskeletal disorders and the global burden of disease study *Ann Rheum Dis* **73** 949–50
- Tran D, Podwojewski F, Beillas P, Ott nio M, Voirin D, Turquier F and Mitton D 2016 Abdominal wall muscle elasticity and abdomen local stiffness on healthy volunteers during various physiological activities *J. Mech. Behav. Biomed. Mater.* **60** 451–9
- Vos T et al 2012 Years lived with disability (ylds) for 1160 sequelae of 289 diseases and injuries 1990–2010: a systematic analysis for the Global Burden of Disease Study 2010 *Lancet* **380** 2163–96
- WHO Scientific Group 2003 *The burden of musculoskeletal conditions at the start of the new millennium* Technical Report Serie 919 World Health Organisation 1–218 Geneva
- Wolf A D and  kesson K 2001 Understanding the burden of musculoskeletal conditions *BMJ* **322** 1079–80
- Yeung F, Levinson S F, Fu D and Parker K J 1998 Feature-adaptive motion tracking of ultrasound image sequences using a deformable mesh *IEEE Trans. Med. Imaging* **17** 945–56

**Supplementary File:**  
**Analytical calculations derived for the paper**  
**“Acousto-elasticity of Transversely Isotropic**  
**Incompressible Soft Tissues: Characterization of**  
**Skeletal Striated Muscle”**

**Jean-Pierre Remeniéras<sup>1</sup>, Michel Destrade<sup>2</sup>**

<sup>1</sup> UMR 1253, iBrain, Université de Tours, Inserm, Tours, France.

<sup>2</sup> School of Mathematics, Statistics and Applied Mathematics, National University of Ireland Galway, University Road, Galway, Ireland.

E-mail: [jean-pierre.remenieras@univ-tours.fr](mailto:jean-pierre.remenieras@univ-tours.fr)

**Abstract.**

This supplementary file details the analytical calculations of the acousto-elasticity method used in the paper “Acousto-elasticity of Transversely Isotropic Incompressible Soft Tissues: Characterization of Skeletal Striated Muscle”. For generality, we treat both the shear-horizontal (SH) and the shear-vertical (SV) propagation modes in homogeneous, transversely isotropic, incompressible solids subject to a uniaxial stress along the fibres. In the main paper, only the results for the (SH) mode are exploited, because our experiments are only sensitive to this polarisation.

Acousto-elasticity requires an expansion of the strain-energy density up to at least the third order in the strain. Here we express the speed of the shear waves as a function of the second- and third-order elastic moduli and of the propagation angle  $\theta$  between the direction of the fibres and the direction of propagation. In the main paper, we take  $\theta = 0^\circ$  and  $\theta = 90^\circ$ , in line with the experiments, but with the expressions calculated in this supplementary file, it is possible to perform a propagation analysis for any angle  $\theta$ , by rotating the probe or by using a 3D Shear Wave Elasticity method.

*Keywords:* Acousto-elasticity theory, Transversely Isotropic soft solid, Third-order elastic constants, Incompressible TI material, strain-energy density.

## 1. Uniaxial stress in incompressible transversely isotropic solids

We model muscles as soft incompressible solids with one preferred direction, associated with a family of parallel fibres, see Figure 1 for a description of the kinematics and physics of the model.

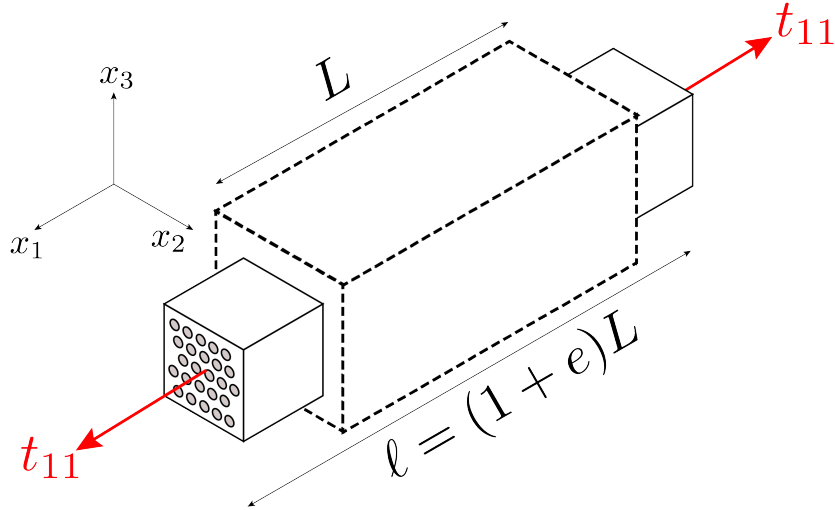


Figure 1: In our experiments, the volunteers apply a uniaxial stress of magnitude  $\sigma_{11}$  along the direction of the fibres (the  $x_1$  axis) during voluntary contractions. In reaction, their muscle experiences the uniaxial Cauchy stress  $t_{11} = -\sigma_{11}$ , and its length is consequently changed by amount  $e$  along  $x_1$ , and by amounts  $-e/2$  along  $x_2$  and  $x_3$  (by symmetry and by incompressibility).

Transversely isotropic (TI), linearly elastic, *compressible* solids are described by five independent constants, for example the following set (Rouze et al., 2020):  $\mu_L, E_L, E_T, \nu_{TT}, \nu_{LT}$ , where  $\mu_L$  is the shear elastic modulus relative to deformations along the fibres,  $E_L, E_T$  are the Young moduli along, and transverse to, the fibres, respectively, and  $\nu_{TT}, \nu_{LT}$  are the Poisson ratios in these directions. The shear elastic modulus  $\mu_T$  relative to the transverse direction is

$$\mu_T = \frac{E_T}{2(1 + \nu_{TT})}. \quad (1)$$

For *incompressible* TI materials, there is no volume change. This constraint leads to the following relations (see Rouze et al. (2020) for details),

$$\nu_{LT} = \frac{1}{2}, \quad \nu_{TT} = 1 - \frac{E_T}{2E_L}. \quad (2)$$

Thus, only three independent constants are required to fully describe a given transversely isotropic, linearly elastic, incompressible solid. Here we choose the three material parameters  $\mu_T, \mu_L$ , and  $E_L$ , as proposed by Li et al. (2016). Other, equivalent choices can be made (Chadwick, 1993; Rouze et al., 2013; Papazoglou et al., 2006), for instance

by using  $\mu_T$ ,  $\mu_L$ , and  $\frac{E_L}{E_T}$ . By inserting  $\nu_{TT}$  given by (2) into (1) we obtain

$$E_L = \left(4\frac{E_L}{E_T} - 1\right)\mu_T, \quad (3)$$

which makes the link between the two descriptions.

As shown in Figure 1, we call  $x_1$  the axis along the fibres and  $t_{11}$  the uniaxial Cauchy stress experienced by the muscle in reaction to the stress  $\sigma_{11}$  applied by the volunteers in that direction during the voluntary contractions. The resulting extension in that direction is  $e$  ( $e > 0$ : elongation,  $e < 0$ : contraction). Then, following Chadwick (1993), we have

$$t_{11} = -p + 2\left(2\frac{E_L}{E_T} - 1\right)\mu_T e, \quad (4)$$

where  $p$  is a Lagrange multiplier introduced by the constraint of incompressibility (to be determined from initial/boundary conditions). Here the lateral stresses are  $t_{22} = t_{33} = 0$  so that

$$0 = -p + 2\mu_T \left(-\frac{e}{2}\right), \quad (5)$$

because the lateral extension is  $-e/2$  by symmetry and incompressibility. This equation yields  $p$  and then,

$$t_{11} = \left(4\frac{E_L}{E_T} - 1\right)\mu_T E_{11}, \quad (6)$$

which can be simplified using (3) into the classical expression  $t_{11} = E_L e$ . In terms of the uni-axial stress  $\sigma_{11} = -t_{11}$  applied by the volunteers on the muscle, we have

$$\sigma_{11} = -E_L e. \quad (7)$$

This relation will be used to go from  $(v - e)$  to  $(v - \sigma_{11})$  formulations of the acousto-elastic equations.

## 2. Third-order expansion of the strain energy in TI incompressible solids

Acousto-elasticity calls for a third-order expansion of the elastic strain energy density  $W$  in the powers of  $\mathbf{E}$ , the Green-Lagrange strain tensor.

For transversely isotropic incompressible solids, the expansion can be written as (Destrade et al., 2010a),

$$W = \mu_T I_2 + \alpha_1 I_4^2 + \alpha_2 I_5 + \frac{A}{3} I_3 + \alpha_3 I_2 I_4 + \alpha_4 I_4^3 + \alpha_5 I_4 I_5, \quad (8)$$

where the second-order elastic constants  $\alpha_1$ ,  $\alpha_2$  are given by

$$\alpha_1 = \frac{1}{2}(E_L + \mu_T - 4\mu_L), \quad \alpha_2 = 2(\mu_L - \mu_T), \quad (9)$$

and  $A$ ,  $\alpha_3$ ,  $\alpha_4$  and  $\alpha_5$  are third-order elastic constants. The strain invariants used in (8) are

$$I_2 = \text{tr}(\mathbf{E}^2), \quad I_3 = \text{tr}(\mathbf{E}^3), \quad I_4 = \mathbf{A} \cdot \mathbf{E} \mathbf{A}, \quad I_5 = \mathbf{A} \cdot \mathbf{E}^2 \mathbf{A}, \quad (10)$$

where  $\mathbf{A}$  is the unit vector in the fibres direction when the solid is unloaded.

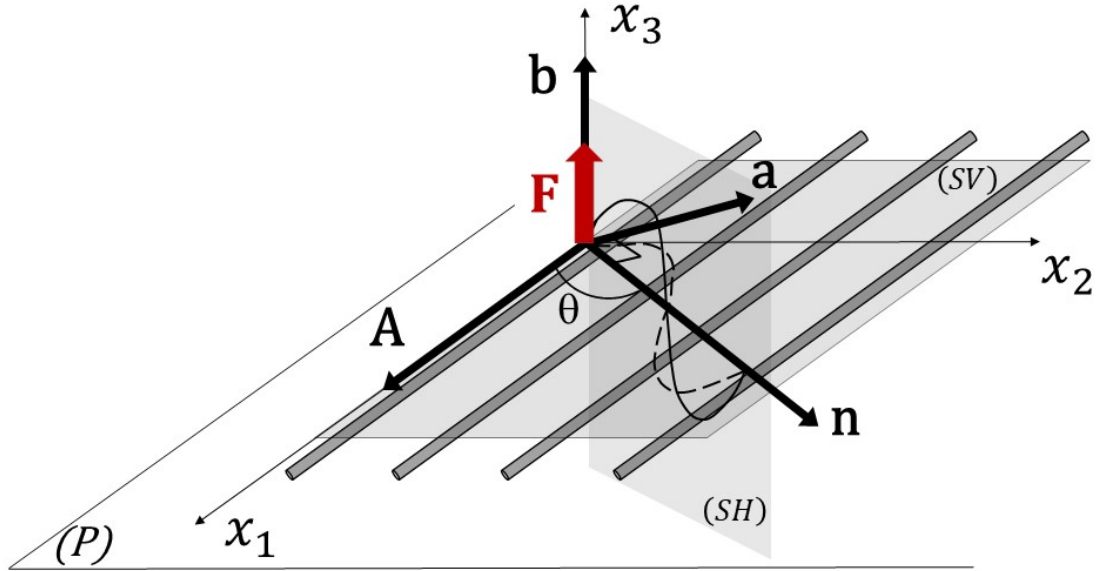


Figure 2: We consider an incompressible transversely isotropic solid under uniaxial stress. Here  $(P)$  is the  $(\mathbf{A}, \mathbf{n})$ -plane where  $\mathbf{A}$  is a unit vector in the fibres direction when the solid is unloaded and at rest, and  $\mathbf{n}$  is a unit vector in the direction of propagation. The uni-axial tensile stress  $\sigma_{11}$  is applied along the fibres. Two purely transverse waves propagate: the shear-vertical (SV) mode with polarization  $\mathbf{a}$  in the  $(\mathbf{A}, \mathbf{n})$ -plane, and the shear-horizontal (SH) mode with polarization  $\mathbf{b}$  normal to the  $(P)$ -plane. We call  $\theta$  the angle between  $\mathbf{n}$  and  $\mathbf{A}$ . In our experiments, the radiation force  $\mathbf{F}$  is applied along the  $x_3$  axis, and we measure the speed of waves travelling along the fibres ( $\theta = 0^\circ$ ) and transverse to the fibres ( $\theta = 90^\circ$ ). Ultrasound tracking measures the  $x_3$  component of the shear wave displacement and is sensitive only to the (SH) propagation mode.

### 3. Small-amplitude plane body waves in the deformed soft tissue

We now consider the propagation of small-amplitude plane body waves in a deformed soft tissue. Destrade et al. (2010a) and Ogden and Singh (2011) show that investigating homogeneous plane wave propagation in TI incompressible solids is equivalent to solving the eigenproblem

$$\overline{\mathbf{Q}}(\mathbf{n}) \mathbf{a} = \rho_0 v^2 \mathbf{a}, \quad (11)$$

where  $\rho_0$  is the (constant) mass density,  $\mathbf{a}$  is the unit vector along the direction of polarisation,  $\overline{\mathbf{Q}}$  is the following symmetric tensor

$$\overline{\mathbf{Q}}(\mathbf{n}) = (\mathbf{I} - \mathbf{n} \otimes \mathbf{n}) \mathbf{Q}(\mathbf{n}) (\mathbf{I} - \mathbf{n} \otimes \mathbf{n}), \quad (12)$$

with  $\mathbf{Q}(\mathbf{n})$  the (symmetric) acoustical tensor. It is defined as

$$[\mathbf{Q}(\mathbf{n})]_{ij} = \mathcal{A}_{0piqj} n_p n_q, \quad (13)$$

where  $\mathcal{A}_0$  is the fourth-order tensor of instantaneous elastic moduli, with components (Destrade et al., 2010a),

$$\mathcal{A}_{0piqj} = F_{p\alpha} F_{q\beta} \delta_{ij} \frac{\partial W}{\partial E_{\alpha\beta}} + F_{p\alpha} F_{q\beta} F_{j\nu} F_{i\gamma} \frac{\partial^2 W}{\partial E_{\alpha\gamma} \partial E_{\beta\nu}}. \quad (14)$$

Here  $W$  is given by (8) and  $\mathbf{F}$  is the deformation gradient.

In our case, the fibres are aligned with the direction of uniaxial stress and elongation, which is along the  $x_1$ -axis in the Eulerian description. Hence, at first-order in  $e$ ,  $\mathbf{F} = \text{Diag}(1 + e, 1 - e/2, 1 - e/2)$ ,  $\mathbf{E} = \text{Diag}(e, -e/2, -e/2)$ ,  $I_4 = e$ ,  $I_5 = 0$ .

Because  $\overline{\mathbf{Q}}(\mathbf{n})$  is symmetric, its eigenvectors are orthogonal. By inspection we see that one eigenvector is  $\mathbf{n}$ , with eigenvalue  $\rho_0 v^2 = 0$  indicating that no longitudinal wave may propagate in perfectly incompressible solids. The other two eigenvectors are  $\mathbf{b} = \mathbf{A} \times \mathbf{n}$ , along  $x_3$ , and  $\mathbf{a} = \mathbf{b} \times \mathbf{n}$  which lies in the (SV) plane. The corresponding two shear velocities are given by

$$\rho_0 v_b^2 = \mathcal{A}_{0piqj} n_p n_q b_i b_j, \quad \rho_0 v_a^2 = \mathcal{A}_{0piqj} n_p n_q a_i a_j. \quad (15)$$

#### 4. Acousto-elasticity of the (SH) wave

The (SH) wave propagates along  $\mathbf{n} = (\cos \theta, \sin \theta, 0)$  and is polarised along  $\mathbf{b} = (0, 0, 1)$ , see Figure 2.

Using (14) and (15), we find that the wave speed  $v_b$  is given by

$$\rho_0 v_b^2 = \gamma_{13} \cos^2 \theta + \gamma_{23} \sin^2 \theta, \quad (16)$$

where

$$\begin{aligned} \gamma_{13} &= \mathcal{A}_{01313} = F_{11}^2 \frac{\partial W}{\partial E_{11}} + F_{11}^2 F_{33}^2 \frac{\partial^2 W}{\partial E_{13}^2}, \\ \gamma_{23} &= \mathcal{A}_{02323} = F_{22}^2 \frac{\partial W}{\partial E_{22}} + F_{22}^2 F_{33}^2 \frac{\partial^2 W}{\partial E_{23}^2}. \end{aligned} \quad (17)$$

We first calculate  $\gamma_{13}$ , using the strain energy  $W$  in (8) and the derivatives formulas of Destrade et al. (2010a). We find, at the first order in  $e$ , that

$$\begin{aligned} \frac{\partial I_2}{\partial E_{11}} &= 2e, & \frac{\partial (I_4^2)}{\partial E_{11}} &= 2e, & \frac{\partial I_5}{\partial E_{11}} &= 2e, \\ \frac{\partial I_3}{\partial E_{11}} &= 0, & \frac{\partial (I_2 I_4)}{\partial E_{11}} &= 0, & \frac{\partial (I_4^3)}{\partial E_{11}} &= 0, \end{aligned} \quad (18)$$

so that

$$F_{11}^2 \frac{\partial W}{\partial E_{11}} = 2(\mu_T + \alpha_1 + \alpha_2) e. \quad (19)$$

The second term in the expression of  $\gamma_{13}$  involves second derivatives of  $W$ . We obtain

$$\begin{aligned} \frac{\partial^2 I_2}{\partial E_{13}^2} &= 1, & \frac{\partial^2 (I_4^2)}{\partial E_{13}^2} &= 0, & \frac{\partial^2 I_5}{\partial E_{13}^2} &= \frac{1}{2}, & \frac{\partial^2 I_3}{\partial E_{13}^2} &= \frac{3}{4}e, \\ \frac{\partial^2 (I_2 I_4)}{\partial E_{13}^2} &= e, & \frac{\partial^2 (I_4^3)}{\partial E_{13}^2} &= 0, & \frac{\partial^2 (I_4 I_5)}{\partial E_{13}^2} &= \frac{1}{2}e, \end{aligned} \quad (20)$$

so that

$$F_{11}^2 F_{33}^2 \frac{\partial^2 W}{\partial E_{13}^2} = \mu_T + \frac{\alpha_2}{2} + \left( \mu_T + \frac{\alpha_2}{2} + \frac{A}{4} + \alpha_3 + \frac{\alpha_5}{2} \right) e. \quad (21)$$

Finally, adding the two expressions, we obtain

$$\gamma_{13} = \mu_T + \frac{\alpha_2}{2} + \left( 3\mu_T + \frac{A}{4} + 2\alpha_1 + \frac{5}{2}\alpha_2 + \alpha_3 + \frac{\alpha_5}{2} \right) e. \quad (22)$$

In terms of the classic linear moduli, see (9), we have

$$\begin{aligned} \gamma_{13} &= \mu_L + \left( E_L + \mu_L - \mu_T + \frac{A}{4} + \alpha_3 + \frac{\alpha_5}{2} \right) e \\ &= \mu_L - \left[ 1 + \frac{1}{E_L} \left( \mu_L - \mu_T + \frac{A}{4} + \alpha_3 + \frac{\alpha_5}{2} \right) \right] \sigma_{11}, \end{aligned} \quad (23)$$

where we used (7) for the latter equality.

Now we compute  $\gamma_{23} = \mathcal{A}_{02323}$ . We find in turn that

$$\frac{\partial I_2}{\partial E_{22}} = -e, \quad \frac{\partial (I_4^2)}{\partial E_{22}} = \frac{\partial I_5}{\partial E_{22}} = \frac{\partial I_3}{\partial E_{22}} = \frac{\partial (I_2 I_4)}{\partial E_{22}} = \frac{\partial (I_4^3)}{\partial E_{22}} = 0, \quad (24)$$

and that

$$\begin{aligned} \frac{\partial^2 I_2}{\partial E_{23}^2} &= 1, & \frac{\partial^2 (I_4^2)}{\partial E_{23}^2} &= 0, & \frac{\partial^2 I_5}{\partial E_{23}^2} &= 0, & \frac{\partial^2 I_3}{\partial E_{23}^2} &= -\frac{3}{2}e, \\ \frac{\partial^2 (I_2 I_4)}{\partial E_{23}^2} &= e, & \frac{\partial^2 (I_4^3)}{\partial E_{23}^2} &= 0, & \frac{\partial^2 (I_4 I_5)}{\partial E_{23}^2} &= 0. \end{aligned} \quad (25)$$

Eventually, we obtain

$$\begin{aligned} \gamma_{23} &= \mu_T - \left( 3\mu_T + \frac{A}{2} - \alpha_3 \right) e \\ &= \mu_T + \frac{1}{E_L} \left( 3\mu_T + \frac{A}{2} - \alpha_3 \right) \sigma_{11}. \end{aligned} \quad (26)$$

We may introduce the non-dimensional coefficients of nonlinearity  $\beta_{\parallel}$  and  $\beta_{\perp}$  used in the main paper, as

$$\begin{aligned} \beta_{\parallel} &= 1 + \frac{1}{E_L} \left( \mu_L - \mu_T + \frac{A}{4} + \alpha_3 + \frac{\alpha_5}{2} \right), \\ \beta_{\perp} &= \frac{1}{E_L} \left( 3\mu_T + \frac{A}{2} - \alpha_3 \right), \end{aligned} \quad (27)$$

to write the *acousto-elasticity equation of (SH) waves* as follows

$$\rho_0 v_b^2 = (\mu_L - \beta_{||} \sigma_{11}) \cos^2 \theta + (\mu_T + \beta_{\perp} \sigma_{11}) \sin^2 \theta, \quad (28)$$

Notice that  $\alpha_4$  does not appear at all in that expression.

In the *isotropic limit*, we have  $\mu_L = \mu_T = \mu$  (the second Lamé coefficient),  $E_L = E_T = 3\mu$ , and  $\alpha_i = 0$ , so that (28) reduces to

$$\rho_0 v_b^2 = \mu + \left[ - \left( 1 + \frac{A}{12\mu} \right) \cos^2 \theta + \left( 1 + \frac{A}{6\mu} \right) \sin^2 \theta \right] \sigma_{11}, \quad (29)$$

in line with the known results of acousto-elasticity (Destrade et al., 2010b; Abiza et al., 2012).

In the *absence of pre-stress*,  $\sigma_{11} = 0$  and (28) reduces to

$$\rho_0 v_b^2 = \mu_L \cos^2 \theta + \mu_T \sin^2 \theta, \quad (30)$$

as expected (Chadwick, 1993). *In vivo* experiments (Gennisson et al., 2003) indeed demonstrate the existence of slow and fast shear waves in the human biceps, as predicted by this relation.

## 5. Acousto-elasticity of the (SV) wave

The (SV) mode has already been studied by Destrade et al. (2010a). Here we write the results in terms of our choice of moduli.

Destrade et al. (2010a) show that the *acousto-elastic equation of (SV) waves* is

$$\rho_0 v_a^2 = \alpha \cos^4 \theta + 2\beta \cos^2 \theta \sin^2 \theta + \gamma \sin^4 \theta, \quad (31)$$

where the parameters  $\alpha$ ,  $\gamma$  and  $\beta$  can be written as follows. Either in terms of  $e$ , as

$$\begin{aligned} \alpha &= \mu_L + \left( E_L + \mu_L - \mu_T + \frac{A}{4} + \alpha_3 + \frac{\alpha_5}{2} \right) e, \\ \beta &= -\mu_L + \frac{1}{2} (E_L + \mu_T) + \left( \frac{5}{2} E_L - \mu_L - 5\mu_T + \frac{A}{4} + 4\alpha_3 + 3\alpha_4 + \frac{5}{2} \alpha_5 \right) e, \\ \gamma &= \mu_L + \left( \mu_L - \mu_T + \frac{A}{4} + \alpha_3 + \frac{\alpha_5}{2} \right) e, \end{aligned} \quad (32)$$

or terms of  $\sigma_{11}$ , as

$$\begin{aligned} \alpha &= \mu_L - \left[ 1 + \frac{1}{E_L} \left( \mu_L - \mu_T + \frac{A}{4} + \alpha_3 + \frac{\alpha_5}{2} \right) \right] \sigma_{11}, \\ \beta &= -\mu_L + \frac{1}{2} (E_L + \mu_T) - \frac{1}{2} \left[ 5 + \frac{1}{E_L} \left( -2\mu_L - 10\mu_T + \frac{A}{2} + 8\alpha_3 + 6\alpha_4 + 5\alpha_5 \right) \right] \sigma_{11}, \\ \gamma &= \mu_L - \frac{1}{E_L} \left( \mu_L - \mu_T + \frac{A}{4} + \alpha_3 + \frac{\alpha_5}{2} \right) \sigma_{11}. \end{aligned} \quad (33)$$

Notice that all the moduli present in the third-order expansion (8) of the strain energy  $W$  appear in the acousto-elasticity equation for (SV) waves (31), although  $\alpha_4$  disappears in the special cases of the principal waves at  $\theta = 0, 90^\circ$ .

In the *isotropic limit*, we have  $\mu_L = \mu_T = \mu$ ,  $E_L = E_T = 3\mu$ ,  $\alpha_i = 0$ , and the relation reduces to

$$\rho_0 v_a^2 = \mu + \left(3\mu \cos^2 \theta + \frac{A}{4}\right) e = \mu - \left(\cos^2 \theta + \frac{A}{12\mu}\right) \sigma_{11}, \quad (34)$$

which recovers known equations when  $\theta = 0, 90^\circ$  (Gennisson et al., 2007; Destrade et al., 2010b).

In the *absence of uniaxial stress*,  $\sigma_{11} = 0$ , and the relation reduces to

$$\rho_0 v_a^2 = \mu_L + (E_L + \mu_T - 4\mu_L) \sin^2 \theta \cos^2 \theta, \quad (35)$$

in agreement with Li et al. (2016) and Li and Cao (2020).

## References

- Z. Abiza, M. Destrade, and R. W. Ogden. Large acoustoelastic effect. *Wave Motion*, 49(2):364–374, 2012.
- P. Chadwick. Wave propagation in incompressible transversely isotropic elastic media I. Homogeneous plane waves. *Proceedings of the Royal Irish Academy.*, pages 231–253, 1993.
- M. Destrade, M. D. Gilchrist, and R. W. Ogden. Third-and fourth-order elasticities of biological soft tissues. *The Journal of the Acoustical Society of America*, 127(4): 2103–2106, 2010a.
- M. Destrade, M. D. Gilchrist, and G. Saccomandi. Third-and fourth-order constants of incompressible soft solids and the acousto-elastic effect. *The Journal of the Acoustical Society of America*, 127(5):2759–2763, 2010b.
- J.-L. Gennisson, S. Catheline, S. Chaffai, and M. Fink. Transient elastography in anisotropic medium: Application to the measurement of slow and fast shear wave speeds in muscles. *The Journal of the Acoustical Society of America*, 114(1):536–541, 2003.
- J.-L. Gennisson, M. Rénier, S. Catheline, C. Barrière, J. Bercoff, M. Tanter, and M. Fink. Acoustoelasticity in soft solids: Assessment of the nonlinear shear modulus with the acoustic radiation force. *The Journal of the Acoustical Society of America*, 122(6):3211–3219, 2007.
- G.-Y. Li and Y. Cao. Backward Mach cone of shear waves induced by a moving force in soft anisotropic materials. *Journal of the Mechanics and Physics of Solids*, 138: 103896, 2020.
- G.-Y. Li, Y. Zheng, Y. Liu, M. Destrade, and Y. Cao. Elastic Cherenkov effects in transversely isotropic soft materials-i: theoretical analysis, simulations and inverse method. *Journal of the Mechanics and Physics of Solids*, 96:388–410, 2016.
- R. W. Ogden and B. Singh. Propagation of waves in an incompressible transversely isotropic elastic solid with initial stress: Biot revisited. *Journal of Mechanics of Materials and Structures*, 6(1):453–477, 2011.

- S. Papazoglou, J. Rump, J. Braun, and I. Sack. Shear wave group velocity inversion in mr elastography of human skeletal muscle. *Magnetic Resonance in Medicine: An Official Journal of the International Society for Magnetic Resonance in Medicine*, 56(3):489–497, 2006.
- N. C. Rouze, M. H. Wang, M. L. Palmeri, and K. R. Nightingale. Finite element modeling of impulsive excitation and shear wave propagation in an incompressible, transversely isotropic medium. *Journal of Biomechanics*, 46(16):2761–2768, 2013.
- N. C. Rouze, M. L. Palmeri, and K. R. Nightingale. Tractable calculation of the Green’s tensor for shear wave propagation in an incompressible, transversely isotropic material. *Physics in Medicine & Biology*, 65(1):015014, 2020.